Hindawi
Journal of Nanomaterials
Volume 2017, Article ID 7340961, 8 pages
https://doi.org/10.1155/2017/7340961

Research Article

Direct Synthesis of MnO_2 Nanorods on Carbon Cloth as Flexible Supercapacitor Electrode

Shuang Xi, Yinlong Zhu, Yutu Yang, and Ying Liu

School of Mechanical and Electronic Engineering, Nanjing Forestry University, Nanjing 210037, China

Correspondence should be addressed to Shuang Xi; shuangxi@hust.edu.cn

Received 4 January 2017; Accepted 2 March 2017; Published 6 April 2017

Academic Editor: Ruiyong Chen

MnO_2 nanorod/carbon cloth (MnO_2/CC) composites were prepared through in situ redox deposition as freestanding electrodes for flexible supercapacitors. The CC substrates possessing porous and interconnecting structures enable the uniform decoration of MnO_2 nanorods on each fiber, thus forming conformal coaxial micro/nanocomposites. Three-dimensional CC can provide considerable specific surface area for high mass loading of MnO_2, and the direct deposition process without using polymeric binders enables reliable electrical connection of MnO_2 with CC. The effect of MnO_2 decoration on the electrochemical performances was further investigated, indicating that the electrode prepared with 40 min deposition time shows high specific capacitance (220 F/g at a scan rate of 5 mV/s) and good cycling property (90% of the initial specific capacitance was maintained after 2500 cycles) in 1 M Na_2SO_4 aqueous solution. This enhanced electrochemical performance is ascribed to the synergistic effect of good conductivity of carbon substrates as well as outstanding pseudocapacitance of MnO_2 nanorods. The obtained MnO_2/CC compositing electrode with the advantages of low cost and easy fabrication is promising in applications of flexible supercapacitors.

1. Introduction

Manganese oxide, as one of the most promising electrode materials for supercapacitors, has attracted significant attention with its excellent electrochemical properties such as high theoretical pseudocapacitance (~1370 F/g), low cost, and environmental friendliness [1, 2]. However, in practice such high theoretical capacitance has never been reached which is mainly caused by its inherent poor electrical conductivity and dense morphology of the oxide [3, 4]. Particularly, when the mass loading of MnO_2 on the electrode is high (which is essential for obtaining high energy density), densely packed MnO_2 enormously reduce the available surface area participating in the electrochemical process and increase the difficulty for electrolyte penetrating into the bulk MnO_2 and thus raise the contact resistance of the electrode [5–7]. All these phenomena remarkably limit kinetics of charge transfer reaction and finally hinder the improvement of specific capacitance. Therefore, a reasonable-structured MnO_2 coating with good electrical connection becomes essential in designing high-performance electrodes for MnO_2-based supercapacitors [8, 9].

To handle these issues, one powerful and straightforward approach is to transfer bulk MnO_2 to nanoscale structures, that is, nanometer-thick thin films, nanosheets, nanorods, and nanotubes [10, 11], and also grow nano-MnO_2 onto highly conductive cores [12–14]. The nanostructured MnO_2 possessing large surface area could significantly enhance the efficiency in utilizing the electrode material, while the conductive backbone on which MnO_2 dispersed can provide electrical pathway through the backbone to MnO_2 to accomplish the charge storage reaction.

Various conductive substrates could be supporting backbones for MnO_2, including the carbon-based materials [15, 16] and various high-conductivity metal oxides [17, 18]. Among them, carbon cloths (CCs) are considered as promising conductive substrates due to their reasonable cost, excellent chemical stability, and 3D porous network texture. The 3D porous architecture not only allows high mass loading of MnO_2 but also facilitates the diffusion of active species and transport of electrons, leading to good electrochemical performance [7, 19]. Additionally, the flexible nature of carbon cloths is advantageous for the fabrication of flexible supercapacitors from the design and packaging perspectives. In

fact, in many subjects of functional materials research the utilization of 3D conductive backbones clearly indicates nano-MnO_2 shell grown on micron-size conductive carbon fibers can be an effective solution for constructing outstanding supercapacitors [12, 20].

In this work, we reported the binder-free integration of large-area MnO_2 nanorods on CCs through a simple electrodeposition method. The one-step synthesized MnO_2/CC electrodes with the advantages of low cost and being easily scalable exhibit considerable electrochemical properties with high specific capacitance and good cycling property, indicating their broad applications in flexible energy storage device.

2. Experimental

2.1. Materials. CC with hydrophilic surfaces was purchased from CeTech Co. Ltd (W0S 1002, Taiwan, China). All chemicals were of analytical grade. Acetone (AR, ⩾ 99.5%), ethanol (AR, ⩾ 99.7%), $MnSO_4{\cdot}H_2O$ (AR, ⩾ 99.0%), and Na_2SO_4 (AR, ⩾ 99.0%) were purchased from Sinopharm Chemical Reagent Co. Ltd (SCR, Shanghai, China) and used as received without any further purification. Deionized (DI) water (18.2 MU cm) from Milli Q was used throughout the entire experiment, and all aqueous solutions were prepared with ultrapure water.

2.2. Synthesis of MnO_2 on Carbon Cloth. The CC substrates were firstly cleaned by sonication sequentially in acetone, ethanol, and DI water for 30 min each. After being dried, an electrochemical deposition process was then conducted to decorate MnO_2 nanostructures onto pristine CC using Autolab electrochemical workstation (PGSTAT-302 N, Eco Chemie B.V. Company, Utrecht, Netherlands) with a three-electrode system. The process was carried out under galvanostatic conditions at the constant current density of 1 mA/cm^2. A precursor solution with equal volume of 0.1 M $MnSO_4{\cdot}H_2O$ and 0.1 M Na_2SO_4 was used as the electrolyte. The cleaned CC was used as working electrode, a platinum wire was used as counter electrode, and KCl-saturated Ag/AgCl was used as reference electrode. The formation of MnO_2 in the electrochemical deposition process occurs via the following reactions [21]:

$$Mn^{2+} + 2H_2O \longrightarrow Mn^{(3+\Delta)} + (1+\Delta)\,e^- \longrightarrow MnO_2 + 4H^+ + 2e^- \quad (1)$$

Briefly, Mn(II) ion is firstly oxidized to the intermediate species of Mn(III) ion, which is thermodynamically unstable, and then disproportionation reaction of Mn(III) ion occurs to generate MnO_2 before Mn(III) ion is reduced to be Mn(II) ion.

By varying the depositing time from 10 min to 50 min, different morphologies of MnO_2 films were obtained. After deposition, these samples were washed with distilled water to eliminate any loosely attached chemical substance and dried naturally, and then the flexible MnO_2/CC electrodes were fabricated. The overall process is scalable.

2.3. Characterization. The morphologies of the samples were characterized by field emission scanning electron microscopy (FESEM, Hitachi, S-4800, Japan) equipped with energy-dispersive X-ray (EDX). The structures of the samples were examined by X-ray diffraction (XRD, Bruker D8 Advance) with Cu-Ka radiation (1.5418 Å) operating at 40 kV, 100 mA. X-ray photoelectron spectroscopy (XPS) was carried out at room temperature in ESCALAB 250 system. Cyclic voltammetry (CV) and electrochemical impedance spectroscopy (EIS) tests were conducted on an Autolab work station in 1 M Na_2SO_4 aqueous solution. Galvanostatic charging/discharging and cycling tests were conducted using a battery measurement system (LAND CT2001A, Wuhan LAND Electronics, Wuhan, China). All the electrochemical experiments were conducted at room temperature.

3. Results and Discussions

3.1. Structural Characterizations. After electrochemical deposition, MnO_2 was successfully decorated onto the surface of CC. Different depositing durations were preset to investigate the morphology variation of the heterostructures. Typical SEM images of the MnO_2/CC with different depositing time are shown in Figure 1, which clearly demonstrate that the well-established nano-MnO_2 has been grown on CC. Figures 1(a), 1(c), 1(e), 1(g), and 1(i) show the carbon fiber after electrochemical deposition of MnO_2 for 10, 20, 30, 40, and 50 min, respectively, while the enlarged SEM images of the corresponding local area are presented in Figures 1(b), 1(d), 1(f), 1(h), and 1(j), respectively. From the magnified SEM images, it can be found that MnO_2 film consists of large quantities of nanorods, which appears to have a rough, uniform, and worm-like shape. With the relatively short electrochemical depositing duration such as 10 min, the CC surface is covered mostly by the MnO_2 particle islands with some carbon fiber surface exposed to the environment (Figures 1(a) and 1(b)). When the depositing duration is prolonged, the MnO_2 particle islands on the surface of the carbon fibers evolve into more compact film. With the depositing time more than 40 min, the carbon fiber is fully covered by dense MnO_2 nanorods as shown in Figures 1(g)–1(j). These results indicate that the morphology of the product can be readily controlled by simply varying the depositing time of MnO_2.

EDX, XRD, and XPS analysis were employed to determine the composition and crystallinity of MnO_2 deposits, as shown in Figure 2, where the typical MnO_2/CC with depositing time of 40 min was chosen as the testing sample. The EDX analysis is conducted to study the chemical composition of the sample, as shown in Figure 2(a), in which C, Mn, and O elements can be detected. Considering that the C element is coming from the CC substrate, the nanostructure obtained by electrochemical deposition is manganese oxide. To explore the chemical structure and phase purity of the as-prepared deposit, XRD was employed as shown in Figure 2(b). Figure 2(b) shows the XRD patterns of the pristine CC and MnO_2/CC composites. Compared with CC, two additional characteristic peaks at 36.9° and 66.3° (marked by black arrows) appear in the pattern of MnO_2/CC composites, which endorse the presence of amorphous birnessite-type MnO_2 (JCPDS, Card number 18-0802). It can be seen that these MnO_2 peaks are broad and unclear, indicating the

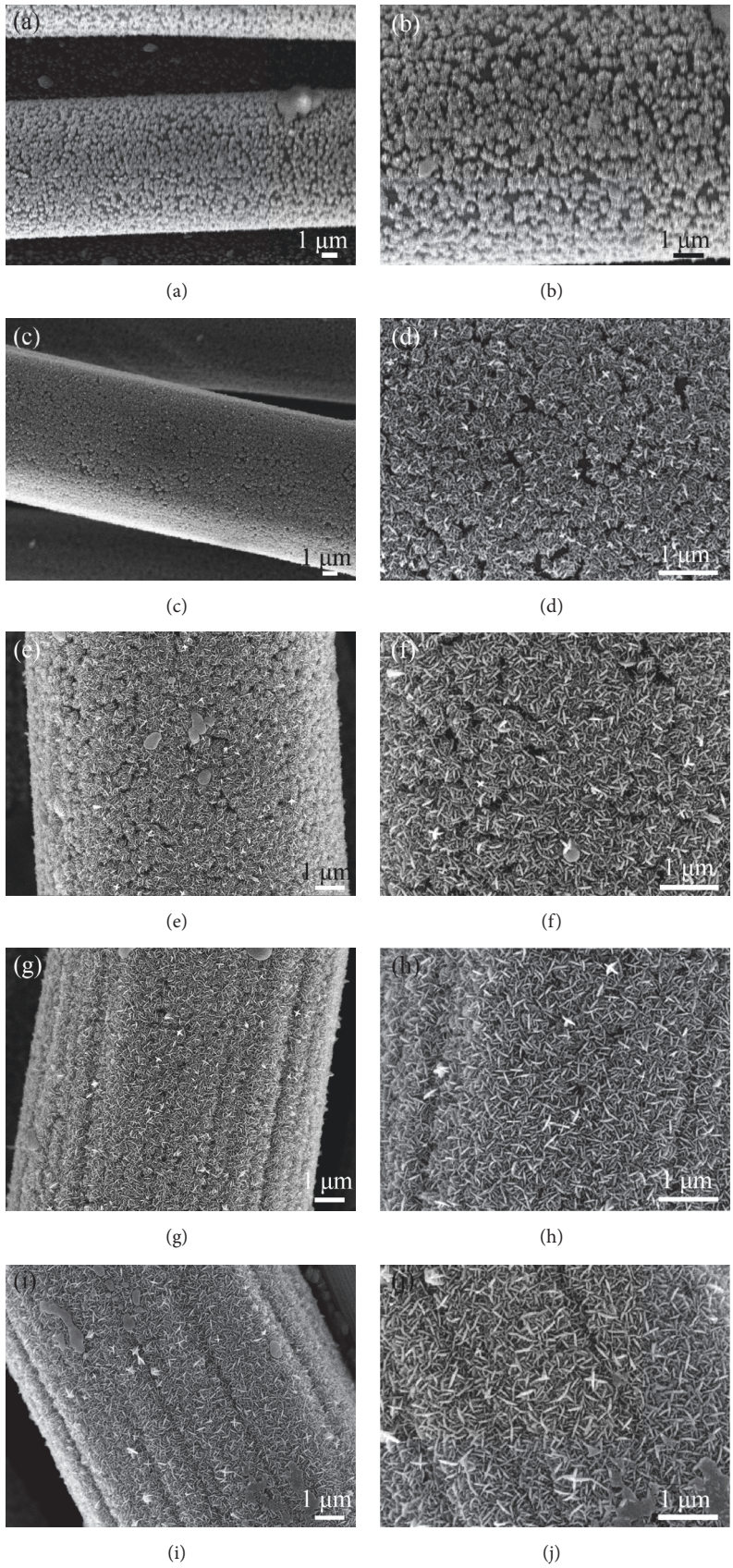

Figure 1: SEM images of MnO_2/CC integrated structures with the left side are low-magnitude views and with the right side are corresponding enlarged views of the left side.

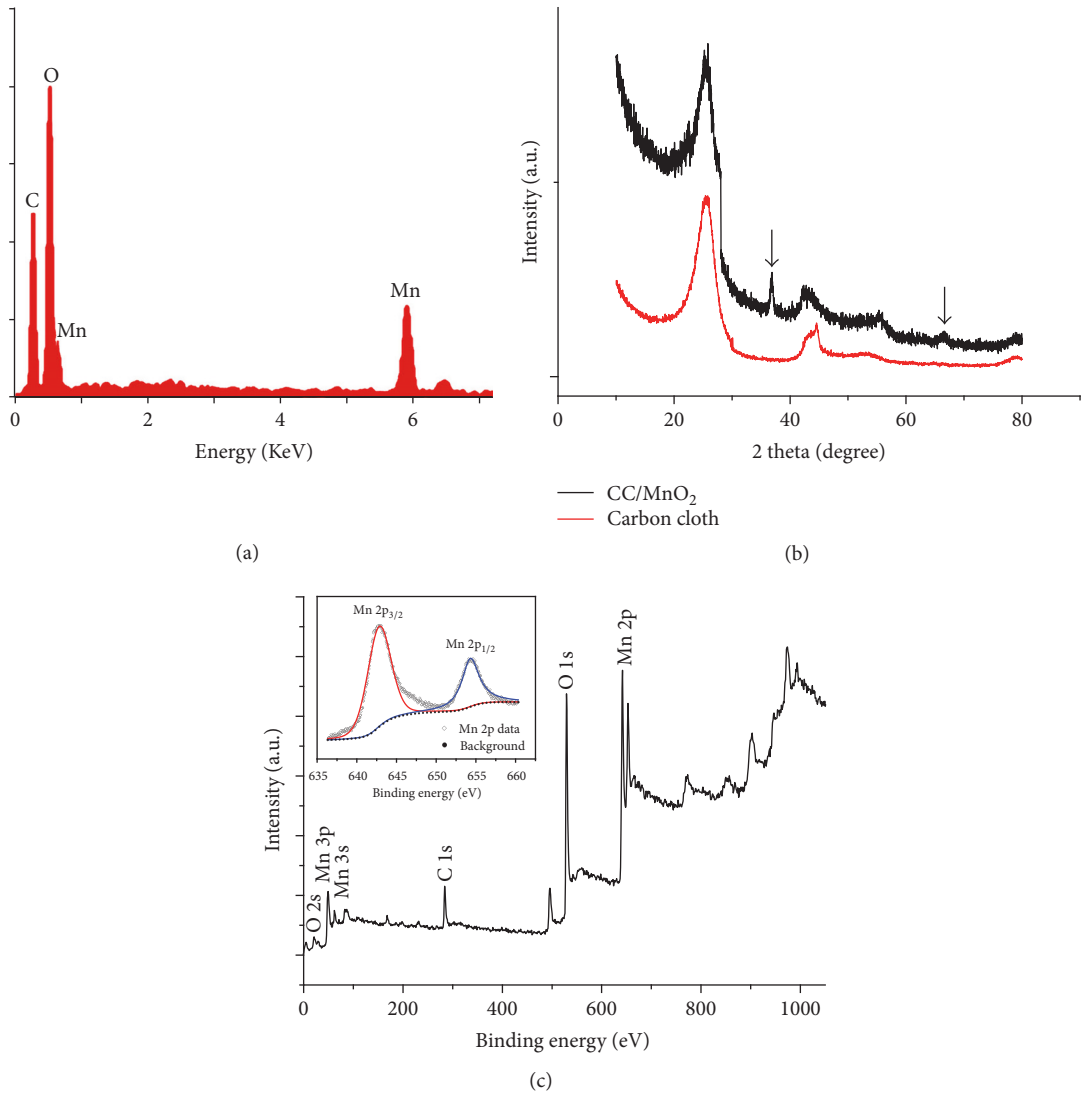

FIGURE 2: (a) EDX spectrums of MnO_2/CC. (b) XRD patterns of MnO_2/CC composites and CC. (c) XPS spectrums of MnO_2/CC with the inset showing the Mn 2p spectrums.

poor crystallinity and fine grain size of the deposition. No extra diffraction peaks other than MnO_2 and carbon were detectable, implying the high purity of the product. From XRD data, the crystallite size of MnO_2 nanoparticles is estimated to be 18.1 nm according to Scherrer's equation.

The sample was further characterized by XPS to investigate the state of Mn within the composites, as shown in Figure 2(c), which exhibits only signals from Mn, C, and O elements, corresponding to the result of EDX. The presence of manganese oxide is evidenced by Mn 3s and Mn 2p peaks along with O 1s and O 2s peaks. As shown in the inset of Figure 2(c), the Mn 2p region consists of a spin-orbit doublet of Mn $2p_{3/2}$ and Mn $2p_{1/2}$ located at 642.7 and 654.3 eV, respectively, with a spin-energy difference of 11.6 eV. These peak values are in good agreement with those reported for MnO_2 [15, 22].

3.2. Electrochemical Evaluations. In order to examine the electrochemical characteristics of the obtained electrodes, samples with size of 1 cm^2 were tested by CV measurements. The specific CV curves of the electrodes are shown in Figure 3(a) with MnO_2 deposition of 0 min (pure CC), 10 min, 20 min, 30 min, 40 min, and 50 min at the scan rate of 50 mV/s in 1 M Na_2SO_4 electrolyte. The CV curves show a near symmetric rectangular shape and exhibit near mirror-image current response on voltage reversal, suggesting a fast, reversible reaction as well as excellent capacitive performance of the hybrid electrode. The specific geometric capacitance of pure CC, due to limited electroactive sites, is as low as 0.0168 mF/cm^2 at the scan rate of 50 mV/s, and the specific geometric capacitance of CC is three magnitudes lower than that of MnO_2/CC. Moreover, after deposition, carbon material underneath is blocked to participate in the charge storage

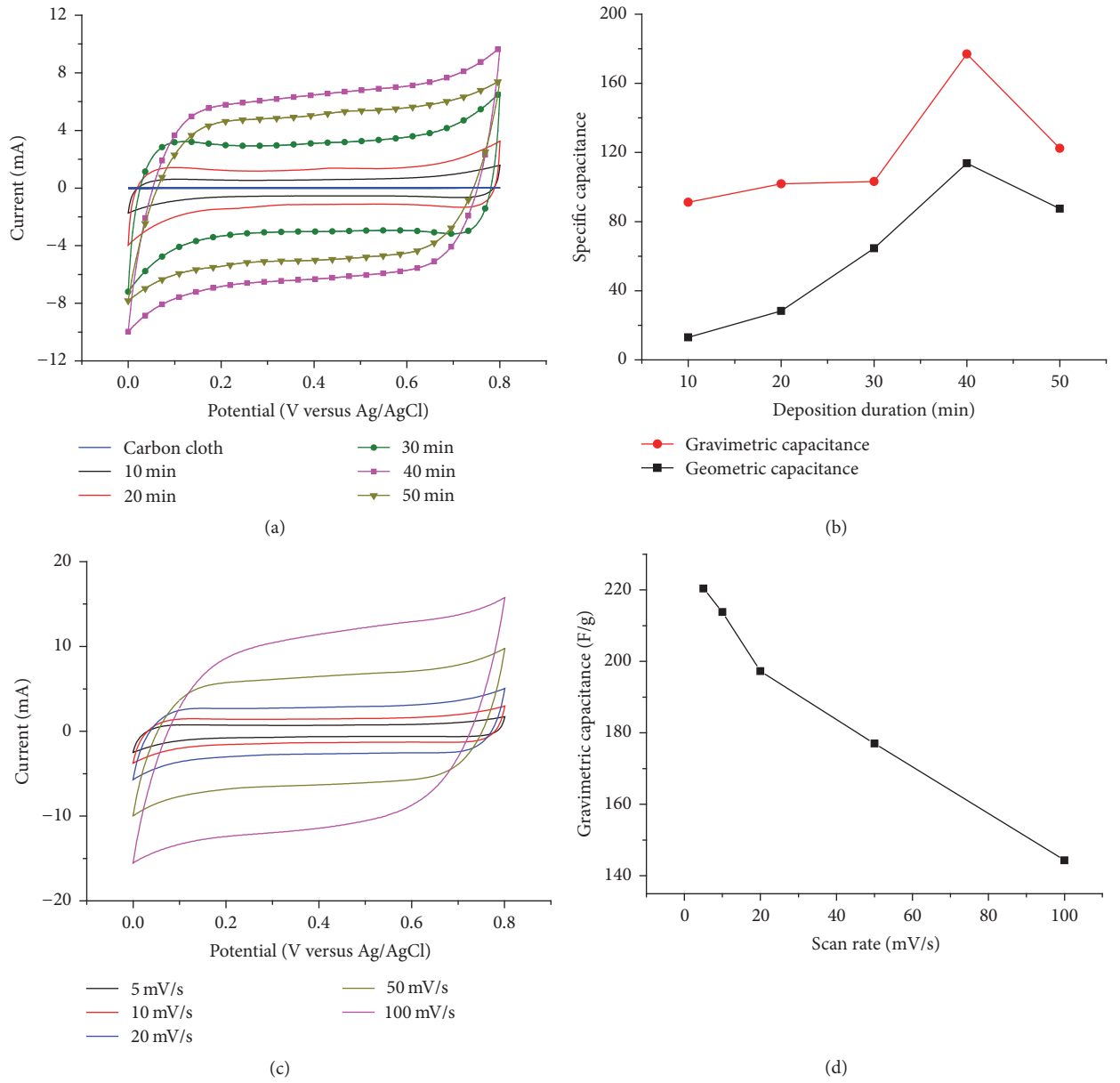

FIGURE 3: (a) CV of the pure CC and MnO_2/CC composites at a scan rate of 50 mV/s in 1 M Na_2SO_4 electrolyte. (b) Gravimetric and geometric capacitance as a function of depositing time. (c) CV of the MnO_2/CC-40 min at various scan rates. (d) Gravimetric capacitance of the MnO_2/CC-40 min as a function of scan rate.

process, considering the process is mainly conducted at or near the surface of the active materials. Hence, the capacitance contribution from carbon core can be negligible to the MnO_2/CC composites.

In Figure 3(a), with short deposition time the CV curves are closer to rectangular shape, while with the deposition time extending CV curves deform gradually. This result is due to the fact that more MnO_2 loading on the carbon surface participating in reactions and thus pseudocapacitance become the main electrochemical mechanism replacing double-capacitance. Moreover, for the depositing time from 10 min to 40 min, the geometric capacitance of MnO_2/CC increases with the depositing time prolonged, while when the depositing duration continues to extend to 50 min, the geometric capacitance decreases (as shown in Figure 3(b)).

As the corresponding mass uptake of MnO_2 increases from 0.146 mg/cm^2 to 0.715 mg/cm^2, the specific gravimetric capacitance depending on the depositing time is plotted in Figure 3(b), in which the same tendency could also be found. That is to say, the specific capacitance of MnO_2/CC rises from 91 F/g (10 min) to 177 F/g (40 min) and then drops to 122 F/g (50 min). This phenomenon can be explained as follows: when the depositing time is less than 40 min, the MnO_2 film could not fully cover the carbon fiber and as the depositing

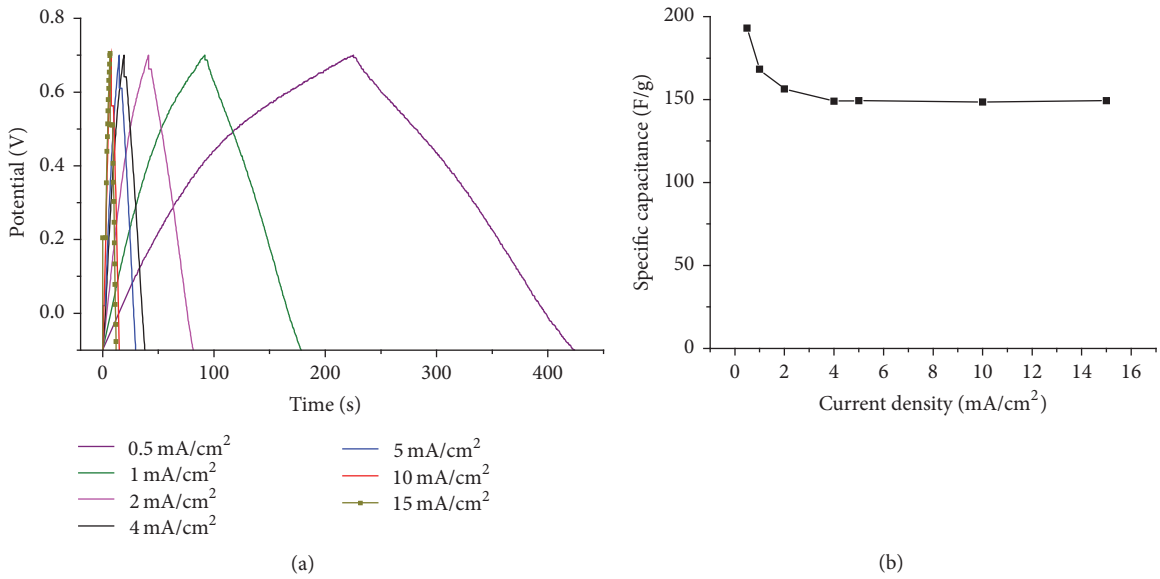

Figure 4: (a) Galvanostatic charging/discharging curves of MnO_2/CC-40 min electrode at different current density. (b) Changing tendency of the specific capacitance depending on current densities.

time increases, the coverage ratio increases apparently (as shown in Figures 1(a)–1(f)); MnO_2 film totally overlays carbon fiber at the depositing time of 40 min (as shown in Figures 1(g)–1(h)), and in this condition, its utilization is most sufficient; when the duration extends to 50 min, MnO_2 loading continues to increase leading the film to be more compacting, which reduces the active site exposing to the electrolyte and thus limits the electrochemical performance of the hybrid electrode. These phenomena reveal that too thick MnO_2 film may limit its optimal electrochemical performance as mentioned earlier. Thus, the employ of MnO_2 film with appropriate thickness and surface morphology is critical to improving the performance of the hybrid electrode, which can be easily controlled by the fabrication process.

The CV curves of the electrodes with 40 min deposition at different scan rates are shown in Figure 3(c). It can be found that the CV shape remains nearly rectangular at a high scan rate of 100 mV/s, indicating a small polarization resistance. As the mass loading of MnO_2 is 0.6428 mg/cm^2 for 40 min depositing process, the calculated specific capacitance is 220 F/g at 5 mV/s and keeps 144 F/g at 100 mV/s scan rate, showing a good rate capability. The dependence of gravimetric capacitance on different scan rate is plotted in Figure 3(d). It is obvious that with the scan rate increasing the specific capacitance decreases substantially. The decline of specific capacitance can be explained as follows: at a low scan rate, the ions in the electrolyte can diffuse sufficiently into the MnO_2 coatings for more charge storage, while at a higher scan rate, the diffusion time is reduced for insertion/extraction of protons or Na^+, leading to a lower capacitance.

The electrochemical performance of MnO_2/CC-40 min electrode was further investigated by galvanostatic charging/discharging technique. Figure 4(a) shows the charging/discharging curves at various current densities from 0.5 to 15 mA/cm^2. It could be observed that the discharge curves are symmetric with their corresponding charge counterparts, indicating superior reversibility and good Coulombic efficiency. These discharge curves are approximately straight line after a small voltage drop (IR drop), which reflects the equivalent series resistance of electrodes, that is, ionic resistance of electrolyte, intrinsic resistance of the hybrid electrode, and interfacial contact resistance between electrode and electrolyte. The specific capacitance obtained from the discharging curves is calculated according to the following equation [9]:

$$C = \frac{I \times \Delta t}{\Delta V \times m}, \tag{2}$$

where I (mA) is the applied current, Δt (s) is the discharge time, ΔV (V) is the sweep potential range, and m (g) is the mass of active material, respectively.

As shown in Figure 4(b), the specific capacitance of MnO_2/CC-40 min decreases distinctly as the current density increases for low current density from 0.5 mA/cm^2 (~193 F/g) to 4 mA/cm^2 (~149 F/g). As the current density continues to increase to 15 mA/cm^2, the areal capacitance drops very little and finally keeps stable (~149 F/g). It is noteworthy that the electrode maintained 77.2% retention of its initial specific capacitance measured at a high rate of 15 mA/cm^2 (23.3 A/g), which is superior to the previously reported values of other MnO_2/carbon-based electrodes including MnO_2/CNT@carbon microelectrode (gravimetric capacitance remains less than 50% with the increase of current density from 0.5 mA/cm^2 to 3 mA/cm^2 [21]), MnO_2/CFP (75% retention from 1 A/g to 10 A/g [23]), and PPy/MnO_2@carbon cloth (capacitance retention of 70% from 0.2 A/g to 5 A/g [24]). Moreover, the specific capacitance of MnO_2/CC-40 min electrode is substantially higher than the value reported for MnO_2 nanosheets/carbon nanofibers (151.1 F/g at the current density of 1 A/g [15]). This suggests that our

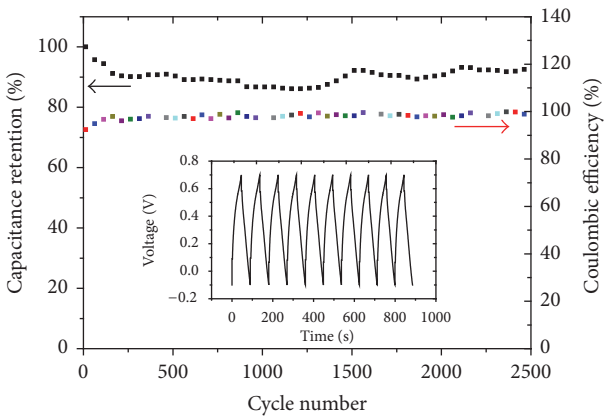

FIGURE 5: Cycling performance and Coulombic efficiency of the electrode up to 2500 cycles at the current density of 2 mA/cm^2. The inset showing the charging/discharging curves after 2000 cycles.

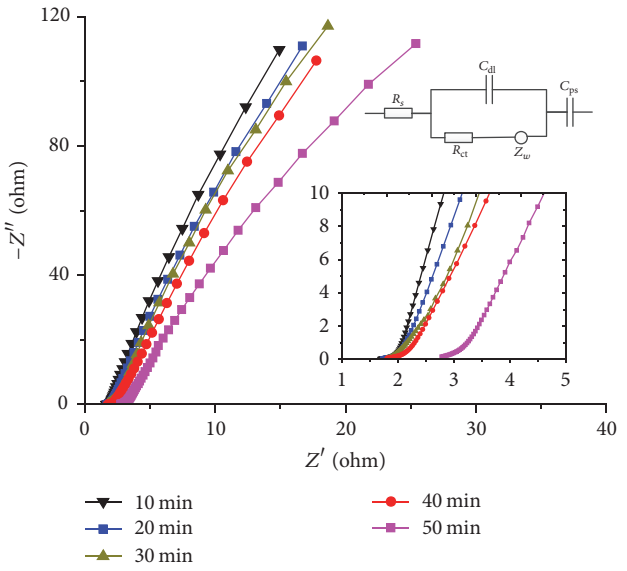

FIGURE 6: Nyquist plots of the MnO_2/CC electrode. The insets are the equivalent circuit and the magnification of Nyquist plots at high frequency.

electrode with its prior feature for fast charge/discharge under a large current density might have huge potential in supercapacitor applications.

Besides high specific capacitance, good cycling performance is also an important property for high-performance supercapacitors. The long-term stability of the MnO_2/CC-40 min electrode was examined through galvanostatic charge/discharge cycling at a current density of 2 mA/cm^2 in 1 M Na_2SO_4 electrolyte. Figure 5 displays the specific capacitance retention and Coulombic efficiency of the hybrid electrode as a function of charge/discharge cycling number. From this figure, the Coulombic efficiency keeps >95% from the 40th cycle and finally reaches to 99%. The capacitance retention decreases about 10% of the initial value over the first 300 cycles, while, then, remaining quite stable for the last 2200 cycles. The inset of Figure 5 shows the last several cycles of charging/discharging curves between −0.1 V and 0.7 V, which exhibit almost the same shape, revealing excellent long-term cyclability of the hybrid array electrode. The excellent cycling performance for MnO_2/CC reveals the good structural stability as well as close contact between MnO_2 nanorods and carbon fibers.

To further understand the fundamental behavior of the prepared supercapacitor electrodes, EIS measurements for MnO_2/CC electrodes with depositing time from 10 min to 50 min have been carried out and the corresponding Nyquist plots are shown in Figure 6. The EIS data can be fitted by an equivalent circuit consisting of internal resistance (R_s), charge transfer resistance (R_{ct}), double-layer capacitance (C_{dl}), pseudocapacitance (C_{ps}), and Warburg impedance (Z_w), as presented in the inset of Figure 6. At high-frequency region, the Nyquist plots of MnO_2/CC-10 min, MnO_2/CC-20 min, MnO_2/CC-30 min, and MnO_2/CC-40 min show similar R_s of 1.68 Ω, 1.70 Ω, 1.77 Ω, and 1.77 Ω, respectively, while MnO_2/CC-50 min has much higher R_s of 2.942 Ω, indicating the MnO_2/CC electrodes with depositing time from 10 min to 40 min possess superior charge transport properties compared with MnO_2/CC-50 min electrode. At low frequency region, the plots of MnO_2/CC electrodes with deposition time from 10 min to 40 min demonstrate steeper Warburg tail, indicating their lower diffusion-resistance. Moreover, C_{ps} for the five electrodes is calculated to be 0.00989 F, 0.01198 F, 0.01239 F, 0.01531 F, and 0.01221 F, respectively, representing the fact that the MnO_2/CC-40 min electrode has the best capacitive property, which could be due to the optimized loading mass of electrochemical active material (MnO_2), and thus providing reasonable active area for electrochemical reactions. All the results suggest that the MnO_2/CC-40 min electrode has very small resistance with good ion response, indicating that the obtained structure could indeed act as a good supercapacitor electrode.

4. Conclusion

In summary, MnO_2 nanorods were successfully synthesized on flexible CC substrates through a facile electrodepositing method. The effect of depositing time on the morphology and electrochemical properties of the composites has been investigated, verifying that the MnO_2/CC electrode with 40 min depositing time demonstrates optimal specific capacitance, good rate capability, and good cyclic stability. Such excellent electrochemical properties are attributed to the synergetic effect of nanostructured MnO_2 and interconnected porous CC acting as a conductive backbone. The prepared electrode may have promising potential as the high-performance flexible supercapacitor.

Conflicts of Interest

The authors declare that they have no conflicts of interest.

Acknowledgments

This work is financially supported by Natural Science Foundation of Jiangsu Province (BK20160934) and National Natural Science Foundation of China (no. 51305209).

References

[1] J. Cao, X. Li, Y. Wang et al., "Materials and fabrication of electrode scaffolds for deposition of MnO_2 and their true performance in supercapacitors," *Journal of Power Sources*, vol. 293, pp. 657–674, 2015.

[2] F. Li, G. Li, H. Chen et al., "Morphology and crystallinity-controlled synthesis of manganese cobalt oxide/manganese dioxides hierarchical nanostructures for high-performance supercapacitors," *Journal of Power Sources*, vol. 296, pp. 86–91, 2015.

[3] M. Huang, R. Mi, H. Liu et al., "Layered manganese oxides-decorated and nickel foam-supported carbon nanotubes as advanced binder-free supercapacitor electrodes," *Journal of Power Sources*, vol. 269, pp. 760–767, 2014.

[4] Z. Lei, J. Zhang, and X. S. Zhao, "Ultrathin MnO_2 nanofibers grown on graphitic carbon spheres as high-performance asymmetric supercapacitor electrodes," *Journal of Materials Chemistry*, vol. 22, no. 1, pp. 153–160, 2012.

[5] M. Huang, F. Li, F. Dong, Y. X. Zhang, and L. L. Zhang, "MnO_2-based nanostructures for high-performance supercapacitors," *Journal of Materials Chemistry A*, vol. 3, no. 43, pp. 21380–21423, 2015.

[6] S. Hassan, M. Suzuki, S. Mori, and A. A. El-Moneim, "MnO_2/carbon nanowall electrode for future energy storage application: effect of carbon nanowall growth period and MnO_2 mass loading," *RSC Advances*, vol. 4, no. 39, pp. 20479–20488, 2014.

[7] P. Lv, Y. Y. Feng, Y. Li, and W. Feng, "Carbon fabric-aligned carbon nanotube/MnO_2/conducting polymers ternary composite electrodes with high utilization and mass loading of MnO_2 for super-capacitors," *Journal of Power Sources*, vol. 220, pp. 160–168, 2012.

[8] Q. Yang, X. T. Zhang, M. Y. Zhang et al., "Rationally designed hierarchical MnO_2-shell/ZnO-nanowire/carbon-fabric for high-performance supercapacitor electrodes," *Journal of Power Sources*, vol. 272, pp. 654–660, 2014.

[9] J.-G. Wang, Y. Yang, Z.-H. Huang, and F. Kang, "Coaxial carbon nanofibers/MnO_2 nanocomposites as freestanding electrodes for high-performance electrochemical capacitors," *Electrochimica Acta*, vol. 56, no. 25, pp. 9240–9247, 2011.

[10] F. Li, Y. X. Zhang, M. Huang, Y. Xing, and L. L. Zhang, "Rational design of porous MnO_2 tubular arrays via facile and templated method for high performance supercapacitors," *Electrochimica Acta*, vol. 154, pp. 329–337, 2015.

[11] M. Huang, Y. Zhang, F. Li et al., "Self-assembly of mesoporous nanotubes assembled from interwoven ultrathin birnessite-type MnO_2 nanosheets for asymmetric supercapacitors," *Scientific Reports*, vol. 4, article 3878, 2014.

[12] M. Yu, T. Zhai, X. Lu et al., "Manganese dioxide nanorod arrays on carbon fabric for flexible solid-state supercapacitors," *Journal of Power Sources*, vol. 239, pp. 64–71, 2013.

[13] S. J. Zhu, J. Zhang, J. J. Ma, Y. X. Zhang, and K. X. Yao, "Rational design of coaxial mesoporous birnessite manganese dioxide/amorphous-carbon nanotubes arrays for advanced asymmetric supercapacitors," *Journal of Power Sources*, vol. 278, pp. 555–561, 2015.

[14] Y. He, S. du, H. Li, Q. Cheng, V. Pavlinek, and P. Saha, "MnO_2/polyaniline hybrid nanostructures on carbon cloth for supercapacitor electrodes," *Journal of Solid State Electrochemistry*, vol. 20, no. 5, pp. 1459–1467, 2016.

[15] P. Ning, X. Duan, X. Ju et al., "Facile synthesis of carbon nanofibers/MnO_2 nanosheets as high-performance electrodes for asymmetric supercapacitors," *Electrochimica Acta*, vol. 210, pp. 754–761, 2016.

[16] H. Li, L. Jiang, Q. Cheng et al., "MnO_2 nanoflakes/hierarchical porous carbon nanocomposites for high-performance supercapacitor electrodes," *Electrochimica Acta*, vol. 164, pp. 252–259, 2015.

[17] Z. Ren, J. Li, Y. Ren, S. Wang, Y. Qiu, and J. Yu, "Large-scale synthesis of hybrid metal oxides through metal redox mechanism for high-performance pseudocapacitors," *Scientific Reports*, vol. 6, Article ID 20021, 2016.

[18] J. Chen, Y. Huang, C. Li, X. Chen, and X. Zhang, "Synthesis of NiO@MnO_2 core/shell nanocomposites for supercapacitor application," *Applied Surface Science*, vol. 360, pp. 534–539, 2016.

[19] Z. Huang, X. Zhao, J. Ren, J. Zhang, Y. Li, and Q. Zhang, "Electrochemical deposition of nanostructured manganese oxide on carbon cloth for flexible high-performance supercapacitor electrodes," *Journal of Nanoscience and Nanotechnology*, vol. 16, no. 6, pp. 5668–5675, 2016.

[20] Y. Luo, J. Jiang, W. Zhou et al., "Self-assembly of well-ordered whisker-like manganese oxide arrays on carbon fiber paper and its application as electrode material for supercapacitors," *Journal of Materials Chemistry*, vol. 22, no. 17, pp. 8634–8640, 2012.

[21] S. Jiang, T. Shi, D. Liu et al., "Integration of MnO_2 thin film and carbon nanotubes to three-dimensional carbon microelectrodes for electrochemical microcapacitors," *Journal of Power Sources*, vol. 262, pp. 494–500, 2014.

[22] L. Li, C. Nan, J. Lu, Q. Peng, and Y. Li, "α-MnO_2 nanotubes: high surface area and enhanced lithium battery properties," *Chemical Communications*, vol. 48, no. 55, pp. 6945–6947, 2012.

[23] M. Yang, S. B. Hong, and B. G. Choi, "Hierarchical MnO_2 nanosheet arrays on carbon fiber for high-performance pseudocapacitors," *Journal of Electroanalytical Chemistry*, vol. 759, pp. 95–100, 2015.

[24] X. Fan, X. Wang, G. Li, A. Yu, and Z. Chen, "High-performance flexible electrode based on electrodeposition of polypyrrole/MnO_2 on carbon cloth for supercapacitors," *Journal of Power Sources*, vol. 326, pp. 357–364, 2016.